POLITECNICO DI TORINO
Repository ISTITUZIONALE

POWER MANAGEMENT SUPPLY OPTIMIZATION FOR HYBRID-ELECTRIC REGIONAL AIRCRAFT

Original
POWER MANAGEMENT SUPPLY OPTIMIZATION FOR HYBRID-ELECTRIC REGIONAL AIRCRAFT / Palaia, G., Abu Salem, K.. - (2024). (34th Congress of the International Council of the Aeronautical Sciences, ICAS 2024 Florence (ITA) 9-13 September 2024).

Availability:
This version is available at: 11583/2997839 since: 2025-02-25T16:18:19Z

Publisher:
International Council of the Aeronautical Sciences

Published
DOI:

Terms of use:

This article is made available under terms and conditions as specified in the corresponding bibliographic description in the repository

Publisher copyright

(Article begins on next page)

26 November 2026



POWER MANAGEMENT SUPPLY OPTIMIZATION FOR HYBRID-ELECTRIC REGIONAL AIRCRAFT

Giuseppe Palaia[1a], Karim Abu Salem[1b]

[1] Mul2 Group, Department of Mechanical and Aerospace Engineering, Politecnico di Torino, Corso Duca degli Abruzzi 24, Torino, Italy

[a]*giuseppe.palaia@polito.it* [b]*karim.abusalem@polito.it*

Abstract

This paper presents a performance analysis of a regional hybrid-electric aircraft equipped with a parallel powertrain. The main focus is given to the role of the power supply split between the electric and thermal power throughout the mission. The performance analysis is carried out by using an in-house design code integrating the main multidisciplinary features of aircraft conceptual design and hybrid-electric propulsion integration. An optimization framework is set up for the identification of the optimal power management strategy, in terms of shares of thermal and electric supplied power in the different stages of the mission; the objective is to minimize the fuel consumption. The power supplied by the thermal engine, modeled as a piecewise function of the time, is considered as an optimization variable; a parametric study on the number of intervals composing this function is performed to search the optimal shape of the power supply profile. The optimization framework is used with a dual purpose: to perform an analysis of the aircraft performance varying range and maximum take-off weight, and to identify the optimal electrical and thermal power profiles to minimize fuel consumption. The results show that hybrid-electric propulsion introduces substantial gains at short ranges, with near-zero fuel consumption up to 400 nm, whereas only a 7.5% fuel reduction is achieved with respect to a full-thermal state of the art reference considering ranges of 800 nm. A simple three-stage profile for the power supply function, i.e. for climb, cruise and descent, has been found as enough to optimize the power split between thermal and electric power for the mission.

Keywords: hybrid-electric propulsion; aircraft design; power management; powertrain optimization; innovation; green aviation

1. Introduction

1.1 Context

The impact of aviation on climate change is well recognized [1],[2], and, according to current projections, this will become much more significant in the near future [3],[4]. In order to significantly reduce the impact of aviation on global warming, several technological advanced solutions are being investigated. Novel and unconventional propulsion systems are under study and development to reduce aircraft emissions, such as hybrid-electric propulsion [5]-[7], hydrogen propulsion [8],[9], high bypass ratio turbofans [10],[11] and innovative engine-airframe integrations such as distributed electric propulsion and boundary layer ingestion [11]-[15]. In addition, innovative airframes such as box-wing [16], truss-braced [17] and blended-wing body [18] are also being investigated for their potentiality to improve aircraft lift-to-drag ratio or exploit unconventional propulsion integration [19]-[21]. All of these technologies aim to introduce a gain over current thermal powered tube-and-wing aircraft with the main target to reduce pollutant and greenhouse emissions. In the field of novel propulsion systems, electric power is reaching the technological maturity to be used for aeronautical applications. However, the well-known limitations imposed by the low gravimetric energy density of batteries [22]-[24] restrict such applications to small aircraft, outside the transport class. To overcome this limitation, today and in the near future, a viable solution is to couple electric power and energy storage systems with thermal ones, in propulsive architectures known as hybrid-electric. This propulsion technology is extensively studied for applications on commuter, see [25],[26], and regional

aircraft, see [27]-[30], whereas applications on larger aircraft may not result in performance benefits, especially in terms of fuel consumption [31]. Conceptual and preliminary studies of regional hybrid-electric aircraft are multiple, and much knowledge on the topic has been disseminated in recent years on the topic [32]-[36]. In general, the characterization of the hybrid-electric aircraft performance requires a deep analysis of the powertrain sizing and the related power supply management throughout the mission. This aspect has been investigated in the literature and several authors have addressed this topic; specifically, techniques such as optimal control, model predictive control and dynamic programming have been used to optimize power supply profile [37]-[44]. In this regard, the main goal is to find the optimal time profile of the power supplied by the electric motors and thermal engines in order to minimize a specific figure of merit, generally the fuel consumption. To do so, the general approach is to model the aircraft as a point mass to derive simplified aircraft dynamics and power equilibrium equations; namely, the latter allows to compute the power supplied by the electric and thermal chains in each time step of the mission. Optimal control, model predictive control and dynamic programming allow to find the optimum time power profile, i.e. the amount of power supplied by electric and thermal chain in each time step of the mission. Generally, the time step is of the order of seconds, whereas the flight mission lasts thousands of second. This aspect highlights that the aforementioned optimization techniques could present high computational cost and are generally not suitable in the early stages of the design process. For more details about the main features of these techniques and their implementation in hybrid-electric aircraft performance assessment, the reader can refer to [45]-[47]. A simpler way to reduce computational cost is to significantly enlarge the time discretization of the simulated mission and to adopt gradient-based algorithm; specifically, the approach used in ref. [48] is based on considering power supply time profile as a piecewise function composed of three stages corresponding to each phase of the mission, namely climb, cruise and descent. The research proposed in ref. [48] highlights the key role of the power management to optimize hybrid-electric aircraft performance; furthermore, as demonstrated in [6] this aspect can not be neglected in the conceptual design process. Similar conclusions emerge from the study proposed in ref. [49] which laid the foundation to the research described in this manuscript, whose main goals are detailed in Section 1.1.

1.2 Aim of the work

This paper proposes a discussion on the performance analysis of regional hybrid-electric aircraft, with the main purpose of identifying the optimal power split profile between thermal and electric sources to minimize the fuel consumption. The management of the power split supply throughout the mission for hybrid-electric aircraft is a crucial aspect that substantially affects overall performance [49]. The different phases of a mission exhibit different power and energy requirements, and allows for different strategy of power utilization: during a low power phase as the taxiing, for example, full-electric power supply enables the suppression of ground noxius emission related to fuel combustion; take-off and climb-out, on the other hand, are typically the most power demanding phases of the mission, thus representing the most stringent requirements for the onboard installed power. Climb, cruise and descent represent less constrained flight phases, allowing the designer wide room to optimise power supply split. Indeed, the preliminary study proposed in ref. [49], based on a 40-seat regional hybrid-electric aircraft which mounts a parallel powertrain, showed that by optimising the power supply split between thermal and electric power for these three mission phases it is possible to achieve substantial performance advantages, expressed as fuel consumption reductions. This paper resumes and expands on what was discussed in [49], investigating the possible effects on powertrain design and performance of a tighter discretization of the mission profile. This investigation serves as a preliminary verification for more advanced insights related to hybrid-electric powertrain control [47]. In fact, several studies have investigated the possibility of designing and optimising closed-loop control systems for electrical and thermal power sources to ensure optimal power supply at all instants of the mission. Throughout the mission, dynamic adjustments could consider real-time and forecasted parameters to achieve the best balance between the power sources supply. As a preliminary step to advanced formulations of control theory, this study aims to identify in advance the potential related benefits, by means of a more simplified formulation of the mission simulation and the power supply time profile.

2. Methodology

2.1 Conceptual design tool

The design and performance analysis of the hybrid-electric aircraft was carried out using the THEA-CODE software [50]. The design framework, shown in Figure 1, combines the main conceptual aircraft design blocks such as aerodynamics, propulsion, flight mechanics and weight estimation. In particular, all the main sub-blocks are inserted in an iterative cycle that terminates when the value of the maximum take-off weight (MTOW) converges under a prescribed tolerance ε.

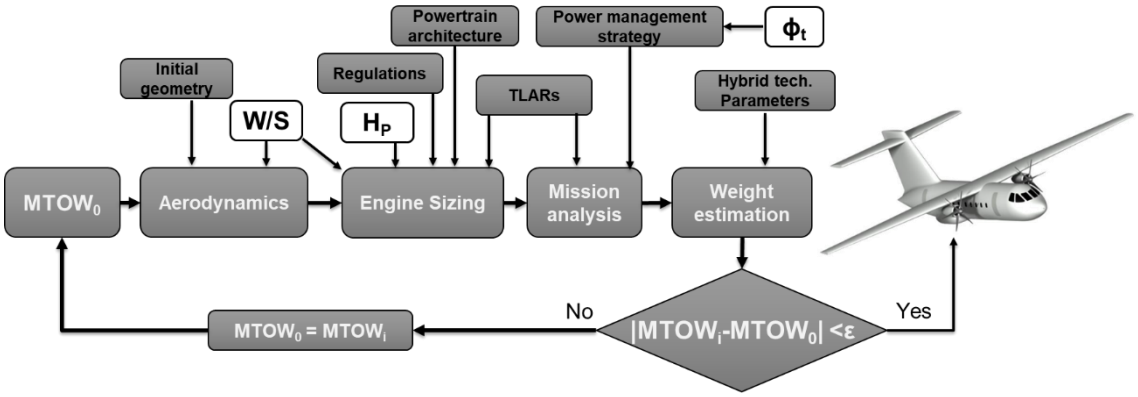


Figure 1 – Design workflow of THEA-CODE.

The selected design variables are the wing loading *W/S*, the degree of hybridization H_P, and the thermal fraction of supplied power Φ_t. The degree of hybridization, defined in accordance with ref. [51], is the ratio between the installed power of the electric motors and the total installed power, calculated as the sum of the installed power of electric motors and thermal engines. The thermal fraction of supplied power is defined as the ratio between the actual power P_t supplied by the thermal engines and the total installed thermal power P_t^i. Generally speaking, Φ_t is a function of time and is directly related to the power supply management strategy. In this design framework it has been considered as a piecewise function; accordingly, the thermal fraction of supplied power of the k-th stage $\Phi_{t,k}$ is defined by Eq. (1):

$$\Phi_{t,k} = \frac{P_{t,k}}{P_t^i} \tag{1}$$

where $P_{t,k}$ is the power supplied by thermal engine at the k-th stage, the superscript *i* refers to the installed power, therefore P_t^i is the thermal engine installed power. The aerodynamics module of the design tool estimates aircraft polar drag by using Vortex Lattice Method (VLM) [52] and a semi-empirical approach [53] to compute induced drag and the parasitic drag, respectively. To define wing geometry during the iterative design process, aspect ratio, taper ratio and sweep angles are kept constant, and the wing surface is homothetically scaled by varying *W/S*. The engine sizing module computes the total installed power according to the current FAR 25 regulations and to the Top-Level Aircraft Requirements (TLARs). It defines specific requirements for each phase of the mission that are plotted in the *P/W-W/S* chart, also named matching chart [54], and allows to calculate the total installed power onboard. The total installed power is split between thermal engine and electric motor according to the value of H_P; if the value of H_P increases, the power allocated to the electric motor raises as well. The mission analysis module computes the aircraft performance by means of the flight simulation, that is largely described in [49]; here, a brief recap is provided. The simulation is set according to the following hypotheses: *i)* the aircraft is a point mass, *ii)* mission trajectory lies in the vertical plane, *iii)* the thrust force is always aligned with the aircraft velocity. Accordingly, Eq. (2-6) describe the motion of the aircraft in the vertical plane during the airborne phases of the mission; W is the aircraft weight, and $\dot{W}$ is its time derivative, L is aircraft lift, P is the required power, D is aircraft drag, V is aircraft speed, γ is flight trajectory angle, P_b is the power supplied by battery pack, k_c is brake-specific fuel consumption, η_t and η_e are the thermal and electric chain efficiency; k_c, η_t and η_e are constant throughout the mission.

$$\dot{W} = -k_c P_t \quad (2)$$
$$L = W \quad (3)$$
$$P = DV + \gamma WV \quad (4)$$
$$P = P_t \eta_t + P_b \eta_e \quad (5)$$
$$P_t = \Phi_t P_t^j \quad (6)$$

The mission is split in different phases, namely taxi-out, take-off, climb, cruise, descent, diversion (composed of climb, cruise and descent), loiter, approach, landing and taxi-in. Regarding the power management, it has been assumed that the electric chain is off during diversion whereas thermal chain is off during taxi operations, as detailed in Table 1. The first choices avoid the need to size the battery pack for an off-design phase; this would have introduced unnecessary weight increases and ineffective gains in terms of emission reduction, as the diversion rarely happens. The second choice, as already stated, allows for the reduction of the ground pollution.

Table 1 – Assumptions on the power management strategy.

Phase	Assumption	Electric chain	Thermal chain
Taxi-out	constant power supply for 240 s	On	Off
Take-off	full-power supply for 45 s	On	On
Climb	constant indicated air speed (IAS) and rate of climb	On	On
Cruise	constant speed and altitude	On	On
Descent	constant indicated air speed (IAS) and rate of descent	On	On
$Climb_{div}$	constant indicated air speed (IAS) and rate of climb	Off	On
$Cruise_{div}$	constant speed and altitude	Off	On
$Descent_{div}$	constant indicated air speed (IAS) and rate of descent	Off	On
Loiter	30 min of level flight at maximum L/D	Off	On
Approach	constant rate of descent	Off	On
Landing	neglected	/	/
Taxi-in	constant power supply for 240 s	On	Off

During the airborne phases of the mission, i.e. climb, cruise and descent, the power is split between thermal and electric chains according to Eq. (5-6). Each airborne phase can in turn be divided in different number of stages, allowing for a more flexible selection of the thermal and electrical power supply profiles; Figure 2 shows an example of a power profile divide in 7 and 16 stages.

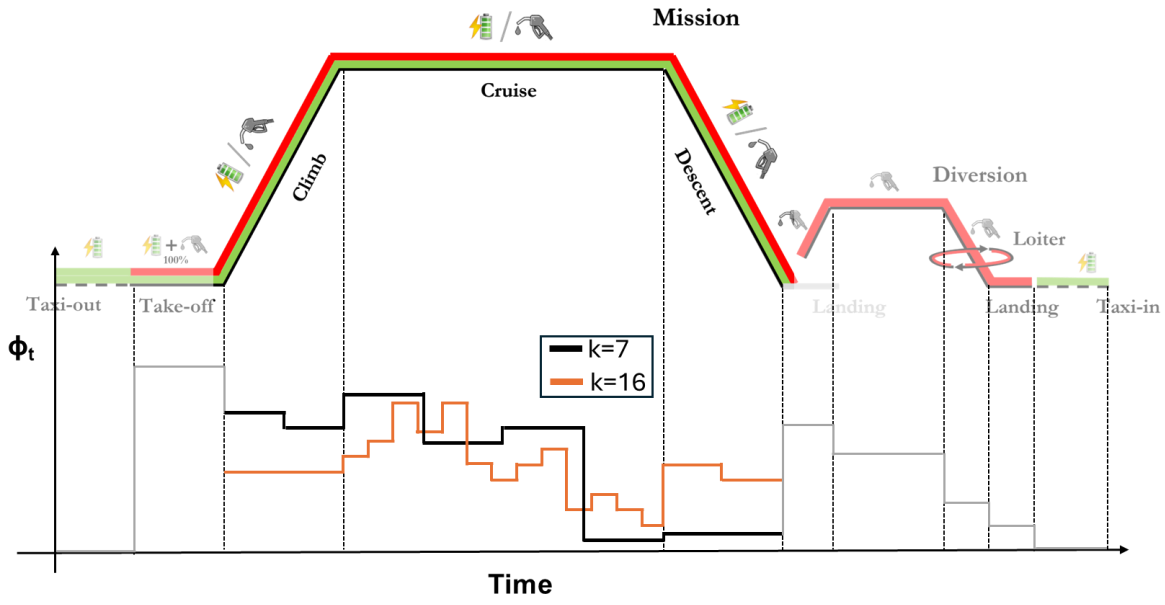


Figure 2 – Examples of Φ_t divided into 7 stages and 16 stages.

The mission analysis block of the design workflow estimates also the weight of the fuel and the battery required to accomplish the mission and diversion; in addition, a reserve fuel and battery mass equal to 5% and 20% of the mass required to accomplish the mission is considered, respectively. The propulsion system weight is evaluated as the ratio between the installed power and the gravimetric density power, for both thermal engines and electric motors [6]. The weight of the other items is evaluated as follows: operating items, furnishing, systems, fuselage, landing gear and tailplanes weights are computed by means of literature models [55], whereas structural lifting system weight is estimated by a FEM-based surrogate model [56][57].

2.2 Optimization framework

The optimization mathematical problem is formulated as follows:

$$\begin{cases} \textbf{objective function} \\ min(FoM(\boldsymbol{x})) \\ \textbf{design space} \\ W/S_{min} < W/S < W/S_{max} \\ 0 < H_P < H_{P_{max}} \\ 0 < \Phi_{t,k} < \varphi_{t,k} \\ \textbf{constraints} \\ MTOW(\boldsymbol{x}) \leq MTOW_{max} \\ \Phi_{e,k} \leq \varphi_{e,k} \end{cases} \tag{7}$$

The objective function, which depends on the vector of the design variables **x**, can be selected in a pool of suitable figure of merits (FoMs), as the block fuel, the block energy, the direct operating cost, the CO_2 emissions, etc., see ref. [58] . The vector **x** is constituted by the design variables reported in Section 2, namely, W/S, H_P and $\Phi_{t,k}$; $\varphi_{t,k}$ and $\varphi_{e,k}$ represent the maximum thermal ad electric fraction of supplied power which can be reached in the k-th stage of the mission. $\varphi_{t,k}$ is computed according to Eq. (8-9):

$$\varphi_{t,k} = \frac{P^a_{t,k}}{P^i_t} \tag{8}$$

$$P^a_{t,k} = \mu_t P^i_t \left(\frac{\rho}{\rho_0}\right)^{0.75} \tag{9}$$

where $P^a_{t,k}$ is the thermal available power at the k-th stage, i.e. the maximum power which can be supplied by the engine at a specific altitude, μ_t is a constraint parameter set to 0.9 to avoid engine overheating, ρ is the air density at a specific altitude, and ρ_0 is the air density at sea level as defined by the ICAO. Climb, cruise and descent are divided into multiple stages which have the same spatial length; accordingly, since the mission profile is fixed a-priori, it is known the altitude of each k-th stage and its corresponding air density. $\Phi_{e,k}$ represents the fraction of electric supplied power, and it is computed by means of Eq. (10-11); η_b, η_{inv} and η_{em} are the battery, inverter and electric motor efficiency, respectively. $P_{e,k}$ and P^i_e are the power supplied by the electric motor at the k-th stage of the mission and the installed electric motor power, respectively. $P_{e,k}$ is computed by Eq. (11) which is related to the value of $\Phi_{t,k}$ and $P_{b,k}$, specifically, by fixing the value of $\Phi_{t,k}$, hence the power supplied by the thermal engines, the power supplied by the electric motors is calculated through Eq. (2-6). Hence, it is sufficient to use $\Phi_{t,k}$ as design variables, and to compute accordingly the univocally related $\Phi_{e,k}$.

$$\Phi_{e,k} = \frac{P_{e,k}}{P^i_e} \tag{10}$$

$$P_{e,k} = P_{b,k}\eta_b\eta_{inv}\eta_{em} \tag{11}$$

The optimization procedure is based on local algorithms coupled with a multi-start approach; in this work n = 10 simulations have been considered for each design case; for more details, the reader can refer to ref. [49]

3. Top-Level Aircraft Requirements and main aircraft data

This section reports the design requirements and assumptions considering a regional hybrid-electric aircraft with an entry into service in 2035. This assumption poses a limitation on the performance of the electric components of the powertrain, whose forecast has been studied and collected in ref. [6], and here assumed as reference for the definition of the electric component main features, reported in Table 2.

Table 2 – Data of the electric components of the powertrain.

Electric powertrain component	Data
Electric motor power density	16 kW/kg
Inverter power density	19 kW/kg
Battery gravimetric energy density	500 Wh/kg
Electric motor efficiency (η_{em})	0.96
Inverter efficiency (η_{inv})	0.98
Battery efficiency (η_b)	0.95

In this study, design requirements similar to those of the ATR 42 have been adopted, as reported in Table 3. The definition of the main parameters of the design mission are reported in Table 4.

Table 3 – Top-Level Aircraft Requirements.

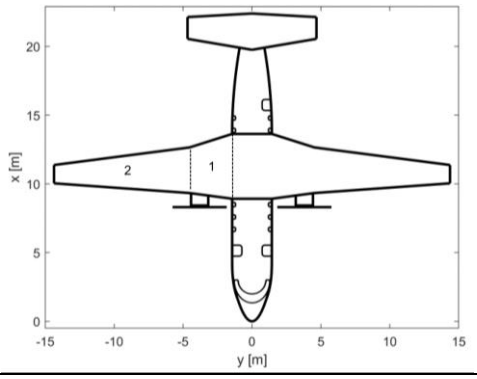
TLARs	
Number of seats	40
Balanced filed length	1100m
Landing distance available	1100m
Cruise condition	M = 0.4 @ FL = 200
Design range	600 nm

Table 4 – Assumptions on the design mission.

Mission phase	Requirement
Climb	IAS = 170 kt rate of climb = 900 ft/min
Cruise	M = 0.4 @ FL = 200
Descent	IAS = 220 kt rate of descent= −1100 ft/min
$Climb_{div}$	IAS = 150 kt rate of climb = 600 ft/min
$Cruise_{div}$	Mach = 0.27 @ FL = 100
$Descent_{div}$	IAS = 150 kt rate of descent= −1100 ft/min

In a similar manner, the geometry of the designed hybrid-electric aircraft resembles the ATR 42; the related main data are reported in Table 5. Regarding the powertrain, the selected architecture is a parallel one.

Table 5 – Main geometrical data of the aircraft.

Aircraft top-view	Parameter	Data
	Fuselage length	21.9 m
	Fuselage cross section diameter	2.88 m
	Wing aspect ratio	11.7
	Wing taper ratio inboard (zone 1)	0.7
	Wing taper ratio outboard (zone 2)	0.4
	Wing sweep angle	6.5°
	Horizontal tail volume coefficient	0.48
	Vertical tail volume coefficient	0.11

4. Results

In this section the main results of the application of the methodology described in Section 2.1 are detailed; specifically, in Section 4.1 a parametric analysis to the design variables is carried out, and the main correlations between the design variables and the block fuel, selected as figure of merit of this work, are discussed. Section 4.2 provides the results of the optimization problem presented in Section 2.2; specifically, the outcomes focuses on the study of the effect of increasing the number of steps in which the power supply profile function is divided: this enables the analysis of the optimal power profile throughout the mission. To provide a quantitative assessment of the performance, a comparison with a reference full-thermal configuration designed by means of the same design methodology is carried out.

4.1 Parametric analysis of the design variables

In this preliminary parametric study, a number of stages equal to two has been considered; this means that Φ_t is constant in two airborne phases of the design mission, namely climb and cruise; to simplify the problem, descent is accomplished by using only thermal power. The chosen values for the parametric analysis are reported Table 6.

Table 6 – Main data of the parametric analysis.

Design parameter	Range
Number of stages	2
W/S [kg_f/m^2]	[255, 265, 275, 285, 295, 305, 315, 325]
H_P	[0.2, 0.25, 0.3, 0.35, 0.4, 0.45, 0.5, 0.55, 0.6]
$\Phi_{t,1}$ (climb)	[0.1, 0.15, 0.2, 0.25, 0.3, 0.35, 0.40]
$\Phi_{t,2}$ (cruise)	[0.1, 0.15, 0.2, 0.25, 0.3, 0.35, 0.40, 0.45, 0.50]

The main outcomes of the parametric study are reported in 2-D plots where the x-axis is the MTOW of the designed configuration (measured in kg_f), and the y-axis is the selected FoM, the block fuel mass m_{fb}. Each point of the chart represents a designed configuration by means of the methodology described in Section 2. The whole group of the configurations designed by combining all the possible design parameters is represented in Figure 3; it can be noticed that there is a wide scatter of the results, and hence it is useful to highlight and discuss the effects of the individual parameters.

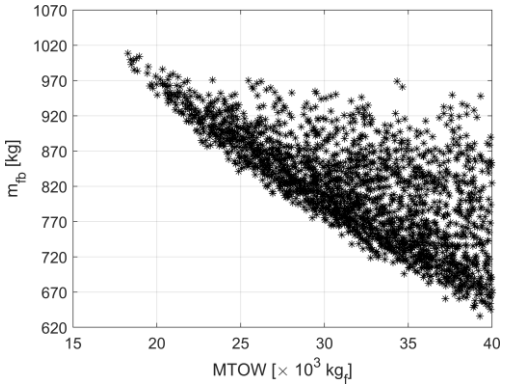


Figure 3 – m_{fb} vs MTOW chart.

The results focusing on the parametric variation of the degree of hybridization H_P are shown in Figure 4; each figure highlights the points that belong to the investigated interval, indicated in the legend, whereas the excluded points are shaded. Two aspects can be noted: i) designed configurations with similar degree of hybridization show a large variability in terms of block fuel; ii) a general trend shows that the higher values of the degree of hybridization (H_P>0.5) could introduce reductions of fuel consumption. Regarding the first point, the great variability of the solutions is due to the fact that just the installed power splitting can not guarantee the achievement of low fuel consumption if a proper power supply management strategy is not provided. The second point is related to the relatively higher installed electrical power; assuming the same parameters Φ of the power management strategy, a configuration designed with a higher degree of hybridization allows a higher electric power supply,

which leads to a reduction in fuel consumption and to an increase of MTOW. This explains why configurations with a higher H_P tend to move towards configurations with higher weight.

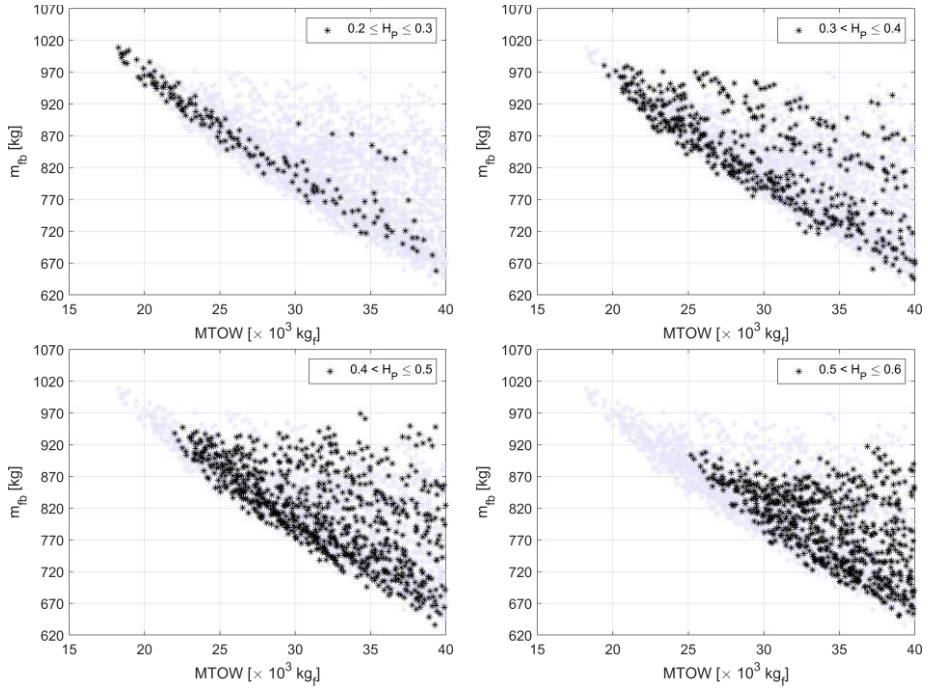


Figure 4 – m_{fb} vs MTOW; configurations with H_P = 0.1-0.2 (top-left); H_P = 0.3 (top-right); H_P = 0.4 (bottom-left); H_P = 0.5 (bottom-right).

Considering the wing loading, Figure 5 top-left highlights that configurations designed with low wing loading, close to the lower bound (see Table 6), exhibit higher fuel consumption than those having high wing loading, cf. Figure 5 bottom-right. Higher wing loading allows for reductions of the wetted surface, and consequently for the increase of the lift-to-drag ratio L/D; if L/D increases, the energy to accomplish the mission decreases, introducing benefits for fuel consumption.

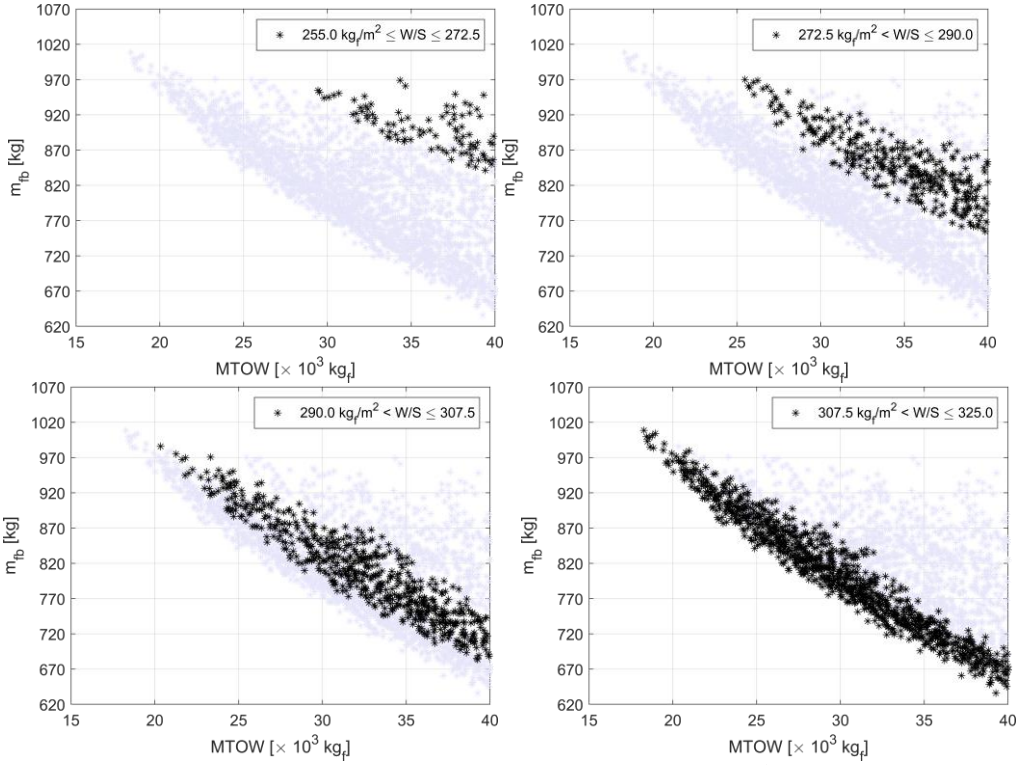


Figure 5 - m_{fb} vs MTOW; configurations with W/S = [255, 272.5] kg_f/m^2 (top-left), W/S = [272.5, 290] kg_f/m^2 (top-right), W/S = [290, 307.5] kg_f/m^2 (bottom-left), W/S = [307.5, 325] kg_f/m^2 (bottom-right).

The results relating to the thermal power supply in cruise $\Phi_{t,2}$ are reported in Figure 6; lower values of $\Phi_{t,2}$ correspond to a higher power supplied by the electric chain in cruise, that is the most energy demanding phase of the mission; this implies a higher request of electrical energy, so of battery mass on board, and this rapidly impacts on the increases of aircraft MTOW. On the other hand, this corresponds to configuration with lower m_{fb}. As the largest amount of fuel consumption occurs during the cruise phase, the same trends are not detectable by only considering the variations of $\Phi_{t,1}$ in climb. The power supply split strategy during the cruise phase represents the key driver to steer the design optimization toward fuel consumption minimization.

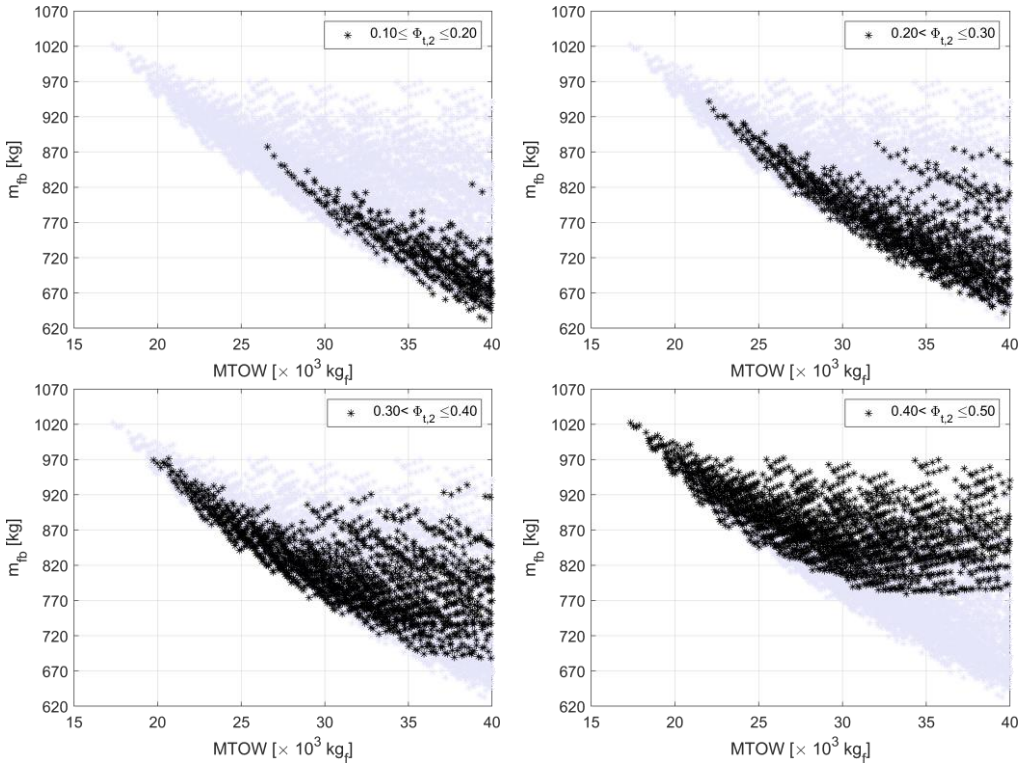


Figure 6 - m_{fb} vs MTOW charts varying thermal power fraction at cruise.

4.2 Optimization results

This section provides the results of different optimizations performed according to the problem defined in Section 2.2, and set according to the indications provided by the parametric study discussed in Section 4.1. First, in Section 4.2.1, the results of the optimization considering a mission split in the basic three stages, i.e. climb, cruise and descent, are discussed. Then, in Section 4.2.2, the effect of increasing the mission stages to accurately optimize the power supply profiles is discussed.

4.2.1 Results of the three-stage mission

In this section the main results related to the discretization of the mission into k = 3 stages is carried out considering the values reported in Table 7 and block fuel as FoM. Each airborne phase of the mission, namely, climb, cruise and descent, has a constant value of Φ_t.

Table 7 – Boundaries assumed for the three-stages analysis.

Variable	Value
W/S_{max}	325 kg/m^2
W/S_{min}	250 kg/m^2
$H_{P_{max}}$	0.7
φ_t	[0.56 0.56 0.56]
φ_e	[1 1 1]
$MTOW_{max}$	23 ×10^3 kg$_f$

Figure 7 shows the results of the optima design variables, namely *W/S*, H_P and Φ_t in climb, cruise, descent, and the related value of block fuel. Each chart presents the statistical analysis of the optima design variables obtained as output of the 10 different multi-start local optimizations, providing a comprehensive overview of the output dataset; the optima values of the design variables are similar in the entire dataset, therefore only the median value is visible in the charts. The results show that wing loading *W/S* is equal to its upper bound for each design case; this result is expected, as detailed in Section 4.1. Regarding the installed power split, almost all the solutions show a degree of hybridization H_P close to 0.40; it means that the thermal chain exhibits a larger share of installed power than the electric chain. Also regarding the power management, it is possible to detect distinct optima values for the three stages, without significant spread. Observing the outcome relating to the figure of merit, all the optimized hybrid-electric solutions has similar block fuel consumption (about 872 kg) which is lower than the thermal reference aircraft of about the 21%.

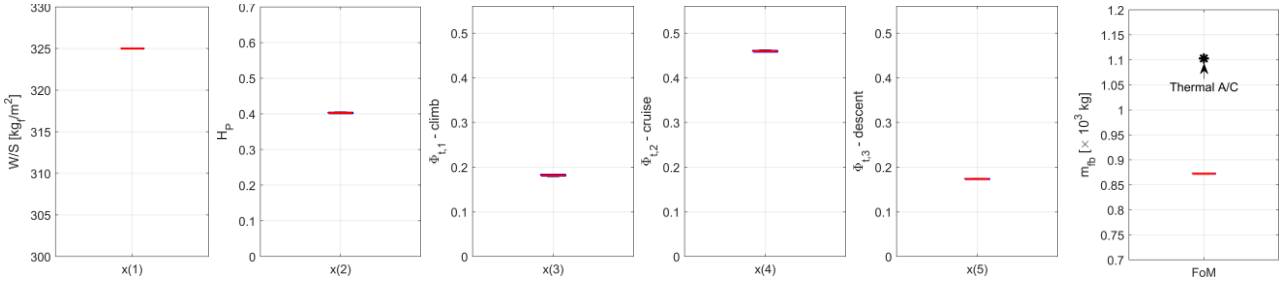


Figure 7 – Statistical analysis of the optima design variables (n=10) and FoM.

To better present the results, the optimum configuration of the dataset in terms of minimum m_{fb} is considered as a reference. Figure 8 highlights the time profiles of the power supplied by thermal engines (left), electric motors (right). As a design choices, to better handle $\Phi_{t,k}$ as design variables, thermal engine supplies constant power in each k-th airborne phase; consequently, the power supplied by the electric motors is an increasing function at climb since the power demand to fly increases; the opposite happens in cruise and descent. The power demand during climb increases due to the flight program defined in Table 4. In cruise phase, the aircraft speed is kept constant, and the power demand reduces due to the reduction of aircraft weight associated to the fuel consumption. During diversion, no electric power is used, as fixed by the designer, see Section 2.1.

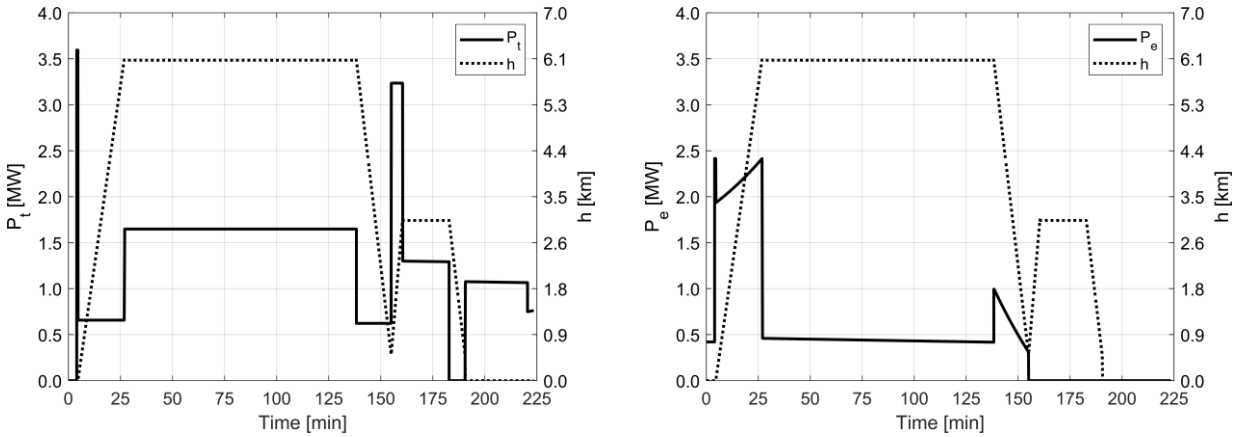


Figure 8 – Power supplied by thermal engines (left) and electric motors (right) vs mission time.

The optimizer finds an electric power supply profile that allows for a reduction of the block fuel consumption of 21% with respect to the thermal reference configuration (described in the Appendix A). However, the electric power supply seems quite limited, especially in the cruise phase, that is the more demanding from an energetic point of view. This is mainly related to the constraint set on $MTOW_{max}$=23 $\times 10^3$ kg_f, that prevent the aircraft to embark a larger battery mass and hence to exploit more electric energy. To discuss this point, an analysis of the optimization output varying the constraint $MTOW_{MAX}$ = [23,30,35,40]x10^3 kg_f is carried out. Figure 9 shows the results of the optima design variables, in terms of statistical analysis of the 10 local optimizations performed for each $MTOW_{MAX}$; these results highlight the main effects of relaxing the constraint on MTOW. Varying the constraint has no effect on the wing loading, as all the optimized configurations exhibit a wing loading equal to the upper bound of the design space, as observed in Section 4.2.1. The degree of

hybridization optima outputs are more dispersed in case of configurations with higher take-off mass, reaching maximum values around 0.64 for configurations with MTOW = 40x10^3 kg$_f$. This variability in the distribution of the installed power split has an impact on the power supply management, that also offers multiple different solutions for the multi-start local optimization. In general, however, considering the fraction of thermal power supplied in cruise, $\Phi_{t,2}$, the effect of relaxing the $MTOW_{MAX}$ constraint is evident, as increasing the MTOW allows for lower $\Phi_{t,2}$, and hence for a more room to carry on board batteries to provide electric energy for this mission stage.

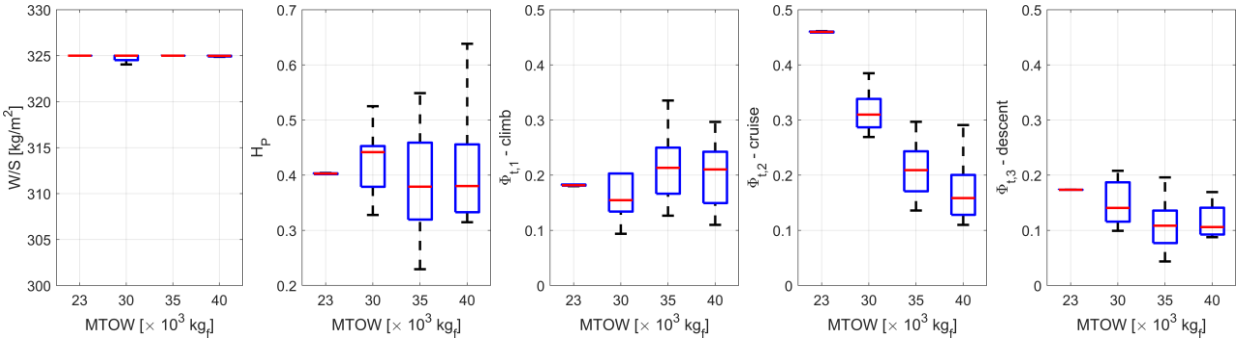


Figure 9 - Statistical analysis of the optima design variables varying $MTOW_{MAX}$.

By enabling the optimizer to design aircraft with a higher MTOW, with the aim of minimizing block fuel consumption, it is possible to find solutions with the highest possible utilization of electrical energy in cruise phase. The battery packs are in fact very heavy and require this relaxation on the MTOW in order to be installed on board. The main data relating to the optima configurations for each MTOW are given in Table 7, and these reveal that the reductions in thermal power supply in cruise (and therefore the corresponding increases in electrical power supply) result in a swap between the energy sources, in the corresponding ratio of their respective gravimetric energy densities. Figure 10 shows that power supplied by electric motors and thermal engines of optima configurations has opposite trends in cruise phase when increasing MTOW.

Table 7 – Main outcomes of the optimizations

Config.	**Design Variables**					**Constraint**	**Obj.**
$MTOW_{MAX}$	**(W/S) [kg$_f$/m^2]**	**H_P**	**$\Phi_{t,1}$**	**$\Phi_{t,2}$**	**$\Phi_{t,3}$**	**MTOW [kg$_f$]**	**m_{fb} [kg]**
23x10^3	325	0.402	0.183	0.459	0.173	23000	872
30x10^3	325	0.525	0.169	0.385	0.184	30000	764
35x10^3	325	0.438	0.151	0.243	0.120	35013	688
40x10^3	325	0.413	0.126	0.180	0.100	40049	620

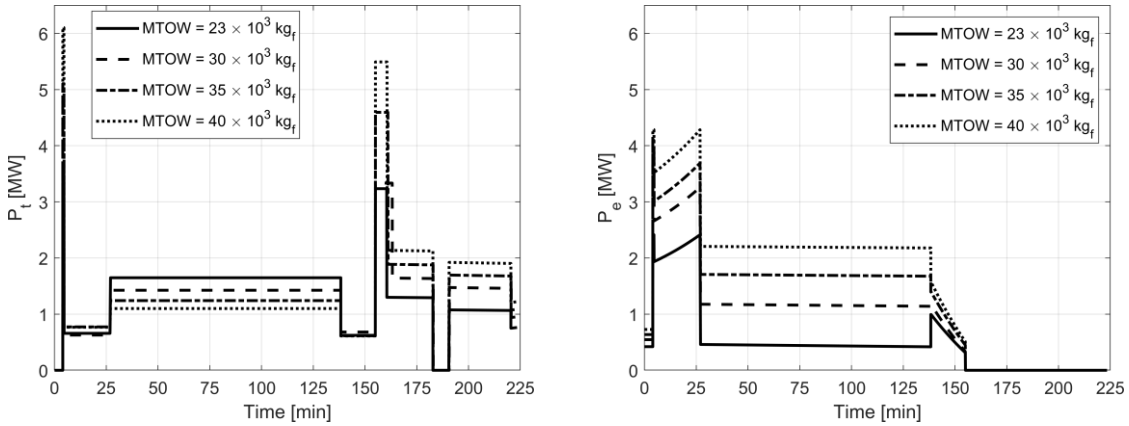


Figure 10 – Mission power profiles varying MTOW: thermal(left) and electric (right).

The comparison with the full-thermal reference configuration is reported in Table 8 and shows that the block fuel consumption reduces up to 44% by relaxing the constraint on MTOW.

Table 8 – Comparison between hybrid-electric and thermal aircraft @600 nm.

Powertrain	W/S [kg_f/m^2]	P_t^i [MW]	P_e^i [MW]	MTOW [kg_f]	m_b [kg]	m_{fb} [kg]
Thermal	325	4.15	0	15731	0	1103 (ref)
Hybrid-electric	325	3.593	2.489	23000	4291	872 (-21%)
Hybrid-electric	325	3.704	4.221	30000	8196	764 (-31%)
Hybrid-electric	325	5.105	4.108	35013	10962	688 (-38%)
Hybrid-electric	325	6.102	4.418	40049	13698	620 (-44%)

Finally, the previous analyses have been extended to design range of 400 nm and 800 nm. The results are depicted in Figure 11, showing that the in case of range of 400 nm the aircraft can reduce fuel consumption up to zero in case of configurations with MTOW = 35000 kg_f, whereas, in case of range of 800 nm there is very limited benefit into increasing the amount of battery mass onboard.

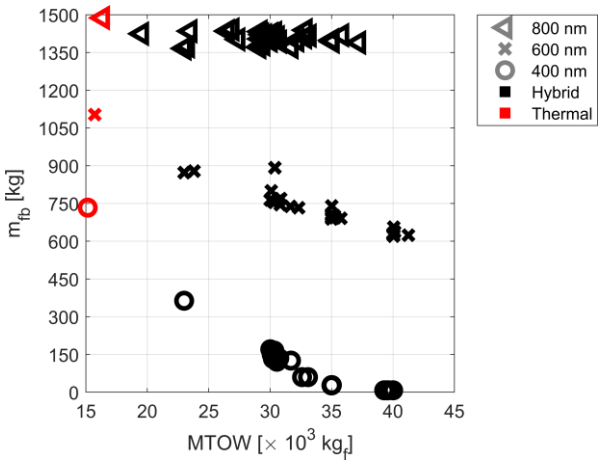


Figure 11 – Block fuel consumption varying range and MTOW.

The results depicted in Figure 11 highlight some interesting aspects related to the design of hybrid-electric regional aircraft: i) the current projections of electric components of the powertrain limits the design range; specifically, the most penalizing factor is the low battery energy density which introduces severe weight increases for longer distances; ii) to introduce noteworthy reductions of fuel consumption, it is necessary to increase aircraft MTOW with respect to the typical values of full-thermal benchmarks. This latter aspect can affect other performance metrics: direct operating cost of aircraft are expected to increase, as already proposed by [34][58], and then also suggested by [59]. Furthermore, aircraft compatibility with airport infrastructure can be a further issue, since to high MTOW is associated a large wingspan which can create compliance issues with apron size. The last two aspects can be mitigated by coupling hybrid-electric powertrain with non-conventional airframe such as the box-wing; in fact, as demonstrated in refs. [27][60], this configuration is able not only to furtherly reduce aircraft fuel consumption, but also to reduce the wingspan for same MTOW of comparable tube-and-wing aircraft, reducing compatibility issues with current apron constraints.

4.2.2 Parametric analysis to the number of stages dividing the mission

In this section a parametric analysis to the number of stages dividing the mission is carried out, assuming the optimization set-up identified by the values reported in Table 7. The selected number of stages, for four different cases considered in this study, is reported in Table 9. The case referred to as "Case 0" represents that studied in Section 4.2.1, the cases referred to as “Case 1”, “Case 2” and “Case 3” consider a different number of stages into climb and cruise; specifically, climb is divided into two stages and cruise into two, four and eight stages, respectively.

Table 9 – Definition of the number of stages for each case.

Phase	Case 0	Case 1	Case 2	Case 3
Climb	1	2	2	2
Cruise	1	2	4	8
Descent	1	1	1	1
n. of stages	3	5	7	11

The main implications occur for the power management strategy. Figure 12-left shows that power fraction supplied by the thermal engine Φ_t increases in the second stage of the climb phase; Figure 12-right shows that the thermal power profile (piecewise function), whereas the electric power profile is a sawtooth function.

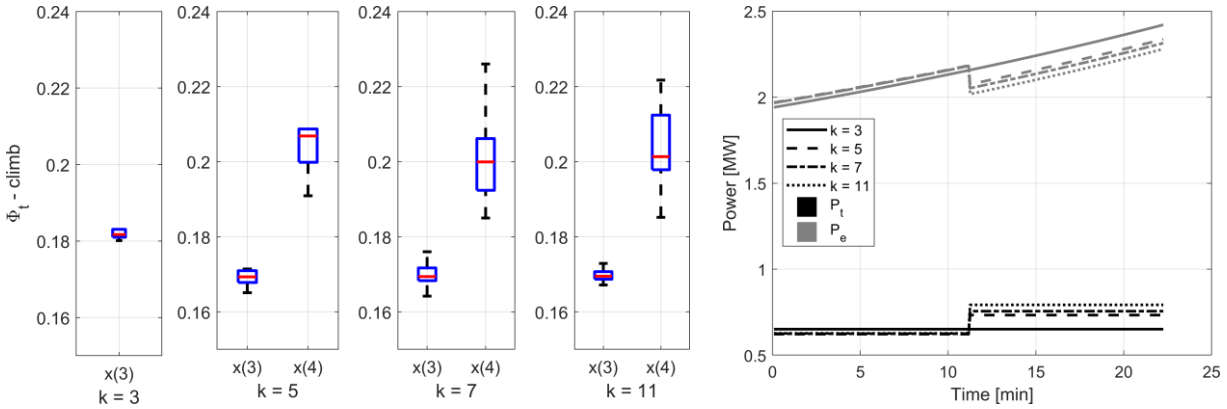


Figure 12 – Optima Φ_t (climb) varying number of stages (left), corresponding power profiles (right).

Figure 13 shows that, increasing the dividing stages of the cruise, the optimizer finds a thermal power supply profile that decreases during cruise; compared to the single-stage cruise case, the solutions steer towards a profile with higher Φ_t at the beginning of the phase, and a lower Φ_t at the end; as shown in Figure 14 for the optima configurations, this reflects in an opposite trend for the electric power fraction.

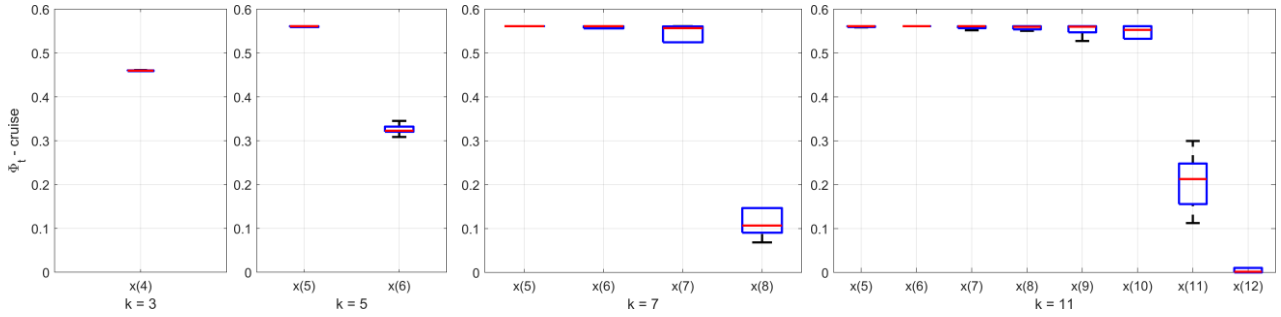


Figure 13 - Thermal power fraction of cruise phase varying the number of stages.

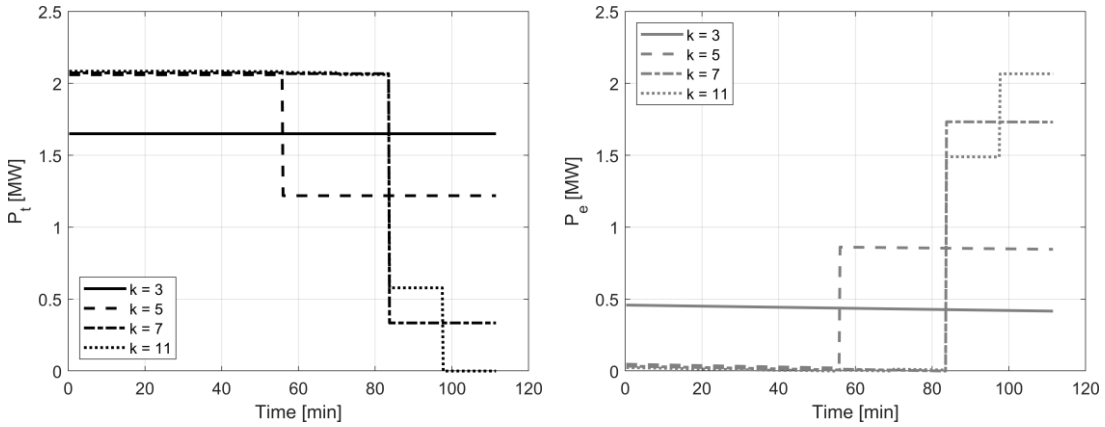


Figure 14 - Power supplied by the thermal engine (left) and electric motor (right) vs time.

Figure 15 shows that powertrain efficiency increases in the last stages of the cruise phase, for cases having more than one cruise dividing stage. Namely, the powertrain efficiency η is defined by Eq. (12), and its average value $\bar{\eta}$ is defined by Eq. (13). Reduction of the powertrain efficiency occurs in case of more power is demanded to the thermal chain, as demonstrated in [6], because the electric power chains exhibit higher individual component efficiencies. Hence, the optimizer having a widened design space (larger number of dividing stages), searches for solutions with higher $\bar{\eta}$. This causes that the energy supplied by the battery pack E_b, calculated by means of Eq. (14) slightly increases, potentially enabling a related fuel saving.

$$\eta = \frac{TV}{P_b + P_f} \tag{12}$$

$$\bar{\eta} = \frac{\eta}{t} \tag{13}$$

$$E_b = \int_0^t P_b dt \tag{14}$$

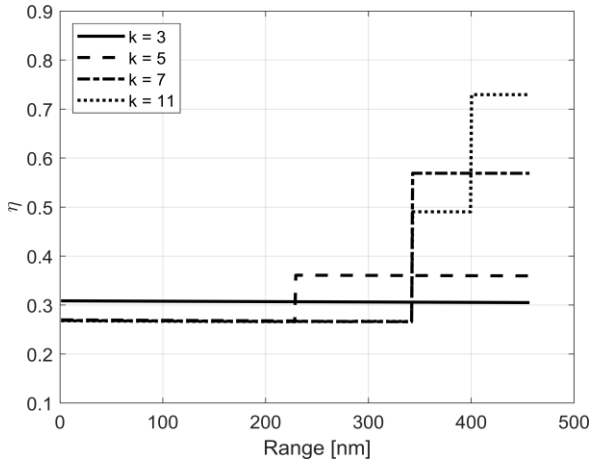


Figure 15 – Powertrain efficiency vs time.

Table 10 summarizes the main outcomes of this explorative study; even if the qualitative trend is that described before, it is evident that the increase in the number of stages does not generate any benefits in terms of reduction of block fuel. In fact, the amount of electric and thermal energy for the optimized aircraft is very similar for all the investigated configurations, and discretizing more in detail the mission power profile is not beneficial for the considered application. These results, together with the general findings commented on in Section 4.2.1, lead to important interrelated conclusions of significant importance in the conceptual design of hybrid-electric aircraft, which we can be summarized as follows: i) the energy gravimetric density limitations of batteries constrain the use of hybrid-electric propulsion on transport aircraft to the regional category only, with tangible performance benefits only on short routes, up to a maximum of 600 nm; ii) optimizing the power supply split, between the electric and thermal chains, is of key relevance to achieve specific performance benefits, such as reduced fuel consumption; iii) given the limited routes length, optimizing the power supply split in the three main mission phases (climb, cruise, descent) is sufficient, while tighter temporal discretization of the power profile would increase the computational cost without providing any additional engineering insights. This enables exploratory studies of such technologies to be done with rather simple models, thereby avoiding the formalization, the implementation, and the computational cost of much more complex simulative models, such as those discussed in refs. [47].

Table 10 –Data of the energy demand to battery and fuel at standard mission.

n. of stages	E_b [kWh]	E [kWh]	m_{fb}	$\bar{\eta}$
3	2084	4471	872	0.493
5	2086	4463	872	0.493
7	2084	4460	870	0.507
11	2090	4463	870	0.509

Focusing more on the technical data proposed in this section, it is worth to underline that the results are also related to the modelling of the powertrain adopted in this work, namely: i) the efficiency of the components of the electric chain is constant and does not depend on the supplied power; ii) the brake specific fuel consumption is constant and does not depend on the power supplied by the thermal engine. These two hypotheses are reasonable in the conceptual design phase since they allow to initialize the design process and to obtain preliminary results, even though some detailed information is not available (e.g. engines performance map). In this regard, the study here proposed showed that, when dealing with the conceptual design of the hybrid-electric aircraft, to minimize a specific figure of merit such as the fuel consumption, assuming that the thermal power fraction is constant in each airborne phase of the mission is sufficiently accurate to achieve a preliminary result to derive key information initialize the preliminary design process.

5. Conclusion

This paper presented a performance analysis of a regional hybrid-electric aircraft equipped with a parallel powertrain. A conceptual multidisciplinary design and optimization framework was used with the dual purpose of identifying the optimal power supply profile to minimise fuel consumption and performing parametric analysis at MTOW and range to assess the impact on aircraft performance. The results showed that: i) the power supply split between electric and thermal chain in the main stages of the missions is a key variable to be handled to optimize the aircraft performance; ii) refining the power profile, by increasing the number of stages dividing the mission, does not provide any benefit; for the airborne mission phases, the ideal number of stages is three, covering climb, cruise and descent, respectively. iii) hybrid-electric propulsion could provide performance gain on short and very-short ranges, while at ranges of 800 nm the benefits in terms of fuel consumption reduction are very limited. For short ranges, furthermore, increasing the MTOW of these aircraft allow for further reductions in fuel consumption, indicating that a trade-off between different performance metrics should be carefully assessed for hybrid-electric aircraft.

6. Appendix

In this section, data of the reference thermal powered tube-and-wing aircraft are presented in Table 11. The aircraft has been developed by using the methodology described in Section 2 according to the TLARs reported in Table 3 and the design mission detailed in Table 4.

Table 11 – Data of the reference thermal aircraft.

	400 nm	**600 nm**	**800 nm**
Wingspan [m]	20.5	20.9	21.4
Fuselage length [m]	21.9	21.9	21.9
Fuselage diameter [m]	2.9	2.9	2.9
Wing aspect ratio	11.7	11.7	11.7
Wing taper ratio inboard	0.7	0.7	0.7
Wing taper ratio outboard	0.4	0.4	0.4
Wing surface [m^2]	46.6	48.2	50.3
Tail surface [m^2]	13	13.5	14
MTOW [kg_f]	15153	15731	16365
OEW [kg_f]	10361	10550	10766
Total fuel (+ reserve) [kg]	1042	1432	1837
Block fuel [kg]	733	1103	1487
Installed power [MW]	4	4.15	4.3

7. Copyright Statement

The authors confirm that they, and/or their company or organization, hold copyright on all of the original material included in this paper. The authors also confirm that they have obtained permission, from the copyright holder of any third party material included in this paper, to publish it as part of their paper. The authors confirm that

they give permission, or have obtained permission from the copyright holder of this paper, for the publication and distribution of this paper as part of the ICAS proceedings or as individual off-prints from the proceedings.

References

[1] Ryley T, Baumeister S and Coulter L. Climate change influences on aviation: A literature review. *Transport Policy*, Vol. 92, pp 55-64, 2020. https://doi.org/10.1016/j.tranpol.2020.04.010

[2] Bows-Larkin A, Mander S L, Traut M B, Anderson K L, Wood F R. Aviation and Climate Change–The Continuing Challenge. *Encyclopedia of Aerospace Engineering*. https://doi.org/10.1002/9780470686652.eae1031

[3] Graver B, Rutherford D, Zhang K. CO2 emissions from commercial aviation: 2013, 2018 and 2019. ICCT, The international council on clean transportation, 2019. Available online: https://theicct.org/publication/co2-emissions-from-commercial-aviation-2013-2018-and-2019/. (accessed on 27/05/2024).

[4] Franz S, Rottoli M and Bertram C. The wide range of possible aviation demand futures after the COVID-19 pandemic. *Environmental Research Letters*, Vol. 17, 2022. Doi: 10.1088/1748-9326/ac65a4,

[5] Brelje B and Martins J. Electric, hybrid, and turboelectric fixed-wing aircraft: A review of concepts, models, and design approaches. *Progress in Aerospace Sciences*, Vol. 104, 2018. https://doi.org/10.1016/j.paerosci.2018.06.004

[6] Abu Salem K, Palaia G and Quarta AA. Review of hybrid-electric aircraft technologies and designs: critical analysis and novel solutions. *Progress in Aerospace Sciences*, Vol. 141, 2023. https://doi.org/10.1016/j.paerosci.2023.100924

[7] Sahoo S, Zhao X and Kyprianidis K. A Review of Concepts, Benefits, and Challenges for Future Electrical Propulsion-Based Aircraft. *Aerospace*, Vol. 44, 2020. https://doi.org/10.3390/aerospace7040044

[8] Adler EJ and Martins JRRA. Hydrogen-powered aircraft: Fundamental concepts, key technologies, and environmental impacts. *Progress in Aerospace Sciences*, Vol. 141, 2023. https://doi.org/10.1016/j.paerosci.2023.100922

[9] Degirmenci H, Uludag A, Ekici S and Karakoc TH. Challenges, prospects and potential future orientation of hydrogen aviation and the airport hydrogen supply network: A state-of-art review. *Progress in Aerospace Sciences*, Vol. 141, 2023. https://doi.org/10.1016/j.paerosci.2023.100923

[10] Magrini A, Benini E, Yao HD, Postma J and Sheaf C. A review of installation effects of ultra-high bypass ratio engines. *Prog. Aerosp. Sci*., Vol. 119, 2020. https://doi.org/10.1016/j.paerosci.2020.100680

[11] Abu Salem K, Palaia G, Bravo-Mosquera PD and Quarta AA. A Review of Novel and Non-Conventional Propulsion Integrations for Next-Generation Aircraft. *Designs*, Vol. 8, 2024. https://doi.org/10.3390/designs8020020

[12] Nicolas G M, Moirou DSS and Panagiotis L. Advancements and prospects of boundary layer ingestion propulsion concepts. *Progress in Aerospace Sciences*, Vol. 138, 2023. https://doi.org/10.1016/j.paerosci.2023.100897.

[13] Fard MT, He J, Huang H and Cao Y. Aircraft Distributed Electric Propulsion Technologies - A Review. *IEEE Transactions on Transportation Electrification*, Vol. 8, No. 4, pp. 4067-4090, 2022. Doi: 10.1109/TTE.2022.3197332.

[14] Bravo-Mosquera PD. Cerón-Muñoz HD, Catalano FM. Design, aerodynamic analysis and optimization of a next-generation commercial airliner. *J. Braz. Soc. Mech. Sci. Eng.*, Vol. 44, pp 1–22, 2022. https://doi.org/10.1007/s40430-022-03924-x

[15] Bravo-Mosquera PD, Cerón-Muñoz HD, Catalano FM. Potential Propulsive and Aerodynamic Benefits of a New Aircraft Concept: A Low-Speed Experimental Study. *Aerospace*, Vol. 10, 2023. https://doi.org/10.3390/aerospace10070651

[16] Abu Salem K, Cipolla V, Palaia G, Binante V and Zanetti D. A Physics-Based Multidisciplinary Approach for the Preliminary Design and Performance Analysis of a Medium Range Aircraft with Box-Wing Architecture. *Aerospace*, Vol. 8, 2021. https://doi.org/10.3390/aerospace8100292

[17] Li L, Junqiang B and Feng Q. Multipoint Aerodynamic Shape Optimization of a Truss-Braced-Wing Aircraft. *J. Aircr.*, Vol. 59, pp. 1179–1194, 2022. https://doi.org/10.2514/1.C036413

[18] Okonkwo P and Smith H. Review of evolving trends in blended wing body aircraft design. *Prog. Aerosp. Sci*. Vol. 82, pp 1–23, 2016. https://doi.org/10.1016/j.paerosci.2015.12.002

[19] Hosseini S, Ali Vaziri-Zanjani M and Reza Ovesy H. Conceptual design and analysis of an affordable truss-braced wing regional jet aircraft. *Proceedings of the Institution of Mechanical Engineers, Part G: Journal of Aerospace Engineering*, Vol. 0, 2020. doi:10.1177/0954410020923060

[20] Cui Z, Lai G, Wang Q, Liang Y and Cao Y. Wind tunnel investigation of different engine layouts of a blended-wing-body transport. *Chinese Journal of Aeronautics*, Vol. 36, pp 123-132, 2023. https://doi.org/10.1016/j.cja.2023.04.027.

[21] Sgueglia, A. Methodology for sizing and optimising a Blended Wing-Body with distributed electric ducted fans. PhD thesis, aéronautique et Astronautique, ISAE-SUPAERO, 2019.

[22] Palaia G, Abu Salem K and Quarta AA. Parametric Analysis for Hybrid–Electric Regional Aircraft Conceptual Design and Development. *Appl. Sci,* Vol. 13, 2023. https://doi.org/10.3390/app131911113

[23] Finger DF, Braun C and Bil C. Impact of battery performance on the initial sizing of hybrid-electric general aviation aircraft. *Journal of Aerospace Engineering*, Vol. 33, 2020. https://doi.org/10.1061/(ASCE)AS.1943-5525.0001113

[24] Viswanathan V, Epstein AH, Chiang YM et al. The challenges and opportunities of battery-powered flight. *Nature*, Vol. 601, pp 519–525, 2022. https://doi.org/10.1038/s41586-021-04139-1

[25] Orefice F, Marciello V, Nicolosi F, Zhang Q, Wortmann G, Menu J and Cusati V. Design of hybrid-electric small air transports. IOP Conference Series: Materials Science and Engineering, Vol. 1226, 2022. http://dx.doi.org/10.1088/1757-899X/1226/1/012075

[26] Salucci F, Trainelli L, Bruglieri M, Riboldi CE, Rolando AL and González GG. Capturing the demand for an electric-

powered short-haul air transportation network, *AIAA SciTech Forum*, Virtual event, 19–21 January, 2021. http://dx.doi.org/10.2514/6.2021-0869

[27]Palaia G, Abu Salem K and Quarta AA. Comparative analysis of hybrid-electric regional aircraft with tube-and-wing and box-wing airframes: a performance study. *Applied Sciences*, Vol. 13, 2023. https://doi.org/10.3390/app13137894

[28]De Vries R, Brown M and Vos R. Preliminary sizing method for hybrid-electric distributed-propulsion aircraft. *Journal of Aircraft*, Vol. 56, 2019. http://dx. doi.org/10.2514/1.c035388

[29]Quibén Figueroa, R., Cavallaro, R., Cini, A., "Feasibility Studies on Regional Aircraft Retrofitted with Hybrid-Electric Powertrains," *Aerospace Science and Technology*, 2024, *in press,* https://doi.org/10.1016/j.ast.2024.109246

[30]Voskuijl M, Van Bogaert J and Rao AG. Analysis and design of hybrid-electric regional turboprop aircraft. *CEAS Aeronautical Journal*, Vol. 9, 2017. http://dx.doi.org/10.1007/s13272-017-0272-1

[31]Abu Salem K, Palaia G, Quarta AA and Chiarelli MR. Medium-Range Aircraft Conceptual Design from a Local Air Quality and Climate Change Viewpoint. *Energies*, Vol. 16, 2023. doi: 10.3390/en16104013

[32]Gesell H, Wolters F and Plohr M. System analysis of turbo-electric and hybridelectric propulsion systems on a regional aircraft. *Aeronaut. J.*, Vol. 123, pp 1602–1617, 2019. http://dx.doi.org/10.1017/aer.2019.61

[33]Finger DF, Braun C and Bil C. Comparative assessment of parallel-hybrid-electric propulsion systems for four different aircraft. *J. Aircr.*, Vol 57, pp 843–853, 2020. http://dx.doi.org/10.2514/1.c035897

[34]Hoelzen J, Liu Y, Bensmann B, Winnefeld C, Elham A, Friedrichs J and Hanke-Rauschenbach R. Conceptual design of operation strategies for hybrid electric aircraft. *Energies*, Vol. 11, pp 1–26, 2018. http://dx.doi.org/10.3390/ en11010217

[35]Antcliff KR, Guynn MD, Marien T, Wells DP, Schneider SJ and Tong MJ. Mission analysis and aircraft sizing of a hybrid-electric regional aircraft. *54th AIAA Aerospace Sciences Meeting*, San Diego, USA, 4–8 January 2016. http://dx.doi.org/10. 2514/6.2016-1028.

[36]Karpuk S and Elham A. Influence of novel airframe technologies on the feasibility of fully-electric regional aviation. *Aerospace*, Vol. 8, pp 1-29, 2021. http://dx.doi. org/10.3390/aerospace8060163

[37]Donateo T, Ficarella A and Spedicato L. Applying Dynamic Programming Algorithms to the Energy Management of Hybrid Electric Aircraft. *ASME Turbo Expo 2018: Turbomachinery Technical Conference and Exposition*, Oslo, Norway, 11–15 June 2018. https://doi.org/10.1115/GT2018-76500

[38]Trawick D, Milios K, Gladin J and Mavris DN. A Method for Determining Optimal Power Management Schedules for Hybrid Electric Airplanes. *AIAA Propulsion and Energy 2019 Forum*, Indianapolis, IN, 19-22 August 2019. https://doi.org/10.2514/6.2019-4500

[39]Doff-Sotta M, Cannon M and Bacic M. Predictive Energy Management for Hybrid Electric Aircraft Propulsion Systems. *IEEE Transactions on Control Systems Technology*, Vol. 31, No. 2, pp. 602-614, 2023. Doi: 10.1109/TCST.2022.3193295

[40]Leite JPSP and Voskuijl M. Optimal energy management for hybrid-electric aircraft. *Aircraft Engineering and Aerospace Technology*, Vol. 92, pp 851–861, 2020. Doi: 10.1108/AEAT-03-2019-0046

[41]Wang W and Koeln JP. Hierarchical Multi-Timescale Energy Management for Hybrid-Electric Aircraft. *ASME 2020 Dynamic Systems and Control Conference*, Virtual event, 5-7 October 2020. https://doi.org/10.1115/DSCC2020-3190

[42]Zhang J, Roumeliotis I and Zolotas A. Nonlinear Model Predictive Control-Based Optimal Energy Management for Hybrid Electric Aircraft Considering Aerodynamics-Propulsion Coupling Effects. *IEEE Transactions on Transportation Electrification*, Vol. 8, No. 2, pp. 2640-2653, 2022. Doi: 10.1109/TTE.2021.3137260.

[43]Wang R and Lukic SM. Dynamic programming technique in hybrid-electric vehicle optimization. *IEEE International Electric Vehicle Conference*, Greenville, USA, 2012. Doi: 10.1109/IEVC.2012.6183284

[44]Misley A, D'Arpino M, Ramesh P and Canova M. A Real-Time Energy Management Strategy for Hybrid-electric Aircraft Propulsion Systems. *AIAA/IEEE Electric Aircraft Technologies Symposium*, Denver, USA, 2021. Doi: 10.23919/EATS52162.2021.9704831

[45]Wang L. *Model Predictive Control System Design and Implementation Using MATLAB®*. Springer Nature, 2009.

[46]Ma Z, Zou S. *Optimal Control Theory The variational method*. Springer Nature, 2020.

[47]Xie Y, Savvarisal A, Tsourdos A, Zhang D and Gu J. Review of hybrid electric powered aircraft, its conceptual design and energy management methodologies. *Chinese Journal of Aeronautics*, Vol. 34, pp 432-450, 2021. https://doi.org/10.1016/j.cja.2020.07.017

[48]Riboldi CED. Energy-optimal off-design power management for hybrid-electric aircraft. *Aerospace Science and Technology*, Vol. 95, 2019. https://doi.org/10.1016/j.ast.2019.105507

[49]Palaia G and Abu Salem K. Mission Performance Analysis of Hybrid-Electric Regional Aircraft. *Aerospace*, Vol. 10, 2023. Doi: 10.3390/aerospace10030246

[50]Palaia G, Zanetti D, Abu Salem K et al. THEA-CODE: A design tool for the conceptual design of hybrid-electric aircraft with conventional or unconventional airframe configurations. *Mechanics and Industry*, Vol. 22, 2021. Doi: 10.1051/meca/2021012

[51]Pornet C and Isikveren AT. Conceptual design of hybrid-electric transport aircraft. *Progress in Aerospace Sciences*, Vol. 79, pp 114-135, 2015. https://doi.org/10.1016/j.paerosci.2015.09.002

[52]Drela M, Youngren H. AVL 3.36 User Primer, Online software manual, Massachusetts Institute of Technology, 2017

[53]Raymer D. *Aircraft Design: A Conceptual Approach, Sixth Edition*. American Institute of Aeronautics and Astronautics (AIAA), 2018, ISBN: 9781600869112

[54]Mattingly JD, Heiser WH and Daley DH. *Aircraft engine design*. American Institute of Aeronautics and Astronautics, Washington, DC, 1987

[55]Wells DP, Horvath BL, McCullers LA. The Flight Optimization System Weights Estimation Method. Tech. Rep. NASA/TM-2017-219627, NASA, 2017

[56]Cipolla V, Abu Salem K, Palaia G, Binante V and Zanetti D. A DoE-based approach for the implementation of structural surrogate models in the early stage design of box-wing aircraft. *Aerosp. Sci. Technol.*, Vol. 117, pp 1-20, 2021. http://dx.doi.org/10.1016/j.ast.2021.106968

[57]Palaia G, Abu Salem K, Cipolla V, Zanetti D and Binante V. A DoE – based scalable approach for the preliminary structural design of Box-Wing aircraft from regional to medium range categories. *AIAA SciTech 2023 Forum*, Maryland, USA, 23–27 January 2023. http://dx.doi.org/10.2514/6.2023-2082.

[58]Abu Salem K, Palaia G. and Quarta AA. Impact of Figures of Merit Selection on the Hybrid-Electric Regional Aircraft Performance Analysis. *Energies*, Vol. 16, 2023. https://doi.org/10.3390/en16237881

[59]Marciello V, Cusati V, Nicolosi F, Saavedra-Rubio K, Pierrat E, Thonemann N and Laurent A. Evaluating the economic landscape of hybrid-electric regional aircraft: A cost analysis across three time horizons. *Energy Conversion and Management*, Vol. 312, 2024. https://doi.org/10.1016/j.enconman.2024.118517

[60]Abu Salem K, Palaia G, Quarta AA. Introducing the Box-Wing Airframe for Hybrid-Electric Regional Aircraft: A Preliminary Impact Assessment. *Appl. Sci.*, Vol. 13, 2023. https://doi.org/10.3390/app131810506